minerals

MDPI

Article

Tectonic Background of Carboniferous to Early Permian Sedimentary Rocks in the East Kunlun Orogen: Constraints from Geochemistry and Geochronology

Xiao Wang [1], Xianzhi Pei [1,2,*], Ruibao Li [1,2], Chengjun Liu [1,2], Lei Pei [1,2], Zuochen Li [1,2], Youxin Chen [1,2] and Meng Wang [1,2]

[1] School of Earth Science and Resources, Chang'an University, Xi'an 710054, China
[2] Key Laboratory of Western China's Mineral Resources and Geological Engineering, Ministry of Education, Xi'an 710054, China
* Correspondence: peixzh@163.com

Abstract: The formation of the East Kunlun Orogen (EKO) was related to the tectonic evolution of the Proto-Tethys and Paleo-Tethys Oceans. However, how the Paleo-Tethys Ocean transited from the Proto-Tethys Ocean, and whether the Paleo-Tethys Ocean subducted northward beneath the East Kunlun–Qaidam Terrane in Carboniferous to Permian times, is still highly debated. Early Carboniferous Halaguole and Late Carboniferous to Early Permian Haoteluowa formations are extensively outcropped in the EKO, north Tibetan Plateau, and have thus recorded key information about the tectonic processes of the Paleo-Tethys Ocean that have implications for the reconstruction of the Northern Paleo-Tethys Ocean (Buqingshan Ocean). Siliciclastic rocks within these formations are collected for petrogeological, geochemical, and detrital zircon U–Pb dating research. Our results show that sandstones from Halaguole and Haoteluowa formations have an average total quartz–feldspar–lithic fragment ratio of $Q_{67}F_{12}L_{21}$ and $Q_{50}F_{20}L_{30}$, respectively, indicating relatively high compositional maturity. The geochemical results suggest that the average values of the Chemical Index of Alteration (CIA) are 57.83 and 64.66; together with their angular to subangular morphology, this indicates that their source rocks suffered from weak weathering and the sandstones are the result of proximal deposition. Geochemical features such as the low La/Th, TiO_2, and Ni values suggest that the parental rocks in the provenance area are mainly acidic igneous rocks with minor intermediate igneous and old sedimentary components. The detrital zircon U–Pb age spectrum of these samples is dominated by age peaks at ~405–503 Ma and ~781–999 Ma, with subordinate age peaks at ~1610–2997 Ma and ~1002–1529 Ma, which show tectono–thermal events similar to those of the North Qimatag Belt (NQB), North Kunlun Terrane (NKT), and South Kunlun Terrane (SKT). These features suggest a contribution from the Early Paleozoic magmatic arc and Proterozoic basements in the NQB, NKT, and SKT to the Halaguole and Haoteluowa formations in these areas. In addition, the youngest zircon age of ~440 Ma from these sandstones is greater than the depositional age of Halaguole and Haoteluowa formations, which is a typical basin depositional feature in a passive continental margin. Geochemical tectonic discrimination diagrams, based on a major and trace element Ti/Zr–La/Sc plot, in combination with a detrital zircon age distribution pattern, all suggest a passive continental margin setting. Considering this together with the previous data, we argue that the Paleo-Tethys Ocean did not begin to subduct northward and that there was no oceanic subduction zone in the south EKO during Carboniferous to Early Permian times. Combining this information with that from previous studies suggests that the initial opening of the Paleo-Tethyan Ocean may have occurred before the Early Carboniferous time, and all the branches of the Paleo-Tethys Ocean constituted a complex ocean–continent configuration across parts of what is now Asia during the Early Carboniferous to Early Permian.

Keywords: East Kunlun Orogen; Carboniferous; Paleo-Tethys Ocean; passive continental margin; detrital zircon U–Pb age; provenance analysis

check for updates

Citation: Wang, X.; Pei, X.; Li, R.; Liu, C.; Pei, L.; Li, Z.; Chen, Y.; Wang, M. Tectonic Background of Carboniferous to Early Permian Sedimentary Rocks in the East Kunlun Orogen: Constraints from Geochemistry and Geochronology. *Minerals* **2023**, *13*, 312. https://doi.org/10.3390/min13030312

Academic Editor: Davide Lenaz

Received: 28 December 2022
Revised: 19 February 2023
Accepted: 21 February 2023
Published: 23 February 2023

Copyright: © 2023 by the authors. Licensee MDPI, Basel, Switzerland. This article is an open access article distributed under the terms and conditions of the Creative Commons Attribution (CC BY) license (https://creativecommons.org/licenses/by/4.0/).

1. Introduction

Detrital zircon, owing to its high closure temperature, as well as good weathering and interference resistance, and the development of micro-analysis techniques, can be analyzed to determine rocks' age distributions, and this method is applied in provenance analysis [1–3]. The U–Pb ages of detrital zircons and whole-rock geochemical features from clastic rocks not only have implications for the nature of the provenance area, and tectonic environment, but also elucidate the evolutionary history of the sedimentary basin and the coupling relationship between the basin and mountain [4–6].

The East Kunlun Orogen (EKO), located in the north Tibetan Plateau, is an important part of the Central China Orogenic Belt (CCOB) [7–10]. It links the West Kunlun Orogen to the west and the Qinling Orogen to the east, and can be subdivided into at least two tectonic evolutionary stages, i.e., one related to the Proto-Tethys Ocean in the Early Paleozoic era and the other related to the Paleo-Tethys Ocean in the Late Paleozoic to Early Mesozoic era [7,8,11–18]. Numerous studies have been carried out on the Early Paleozoic tectonic evolution of the EKO. However, Late Paleozoic to Early Mesozoic tectonic processes are poorly understood, especially the ocean–continent framework of the Paleo-Tethys Ocean during Carboniferous to Permian times, which are still debated. There are two diametrically contrasting tectonic models for the Carboniferous Ocean–continent framework, namely a subduction zone model [7,8,19] and a passive continental margin model [10,20–27]. Most studies have mainly focused on the geochronology and geochemistry of magmatic rocks, and few on Late Paleozoic sedimentary rocks, especially Carboniferous to Permian successions, have been conducted.

In this study, we present new data including petrology, whole-rock geochemistry, and detrital zircon U–Pb geochronology for sandstones from the Lower Carboniferous Halaguole and Upper Carboniferous to Lower Permian Haoteluowa formations in the south EKO. Our study indicates that these Carboniferous to Early Permian sedimentary rocks were formed in a passive continental margin. Combined with previous work, we agree that the Paleo-Tethys Ocean was in a spreading stage with no subduction during the Carboniferous to Early Permian. These new insights would significantly improve our understanding of the Late Paleozoic tectonic history of the Paleo-Tethys Ocean in the EKO.

2. Geological Setting

The E–W-trending EKO is located in northwest China and bounded by the Qaidam Block to the north, the Bayanhar Terrane to the south, the Qinling Orogen Belt to the southeast, and the western Kunlun Orogenic Belt to the west. It is tectonically divided into four tectonic units: the North Qimatag Belt (NQB), the North Kunlun Terrane (NKT), the South Kunlun Terrane (SKT), and the Bayanhar Terrane by the Qimatage–Xiangride suture, central Kunlun suture, and Muztagh–Buqingshan suture from the north to the south [7–10,18,28] (Figure 1b).

The Paleoproterozoic Jinshuikou Group and the Mesoproterozoic Binggou Group make up the Precambrian metamorphic basement of the NKT. The Jinshuikou Group is dominated by paragneisses, migmatites, amphibolites, marbles, and local granulites and eclogites [29–31]. The Binggou Group, unconformably overlying on the Jinshuikou Group, predominantly consists of low-grade metamorphic carbonate and clastic rocks. In addition, Neoproterozoic gneissic granite and Paleozoic granitic intrusions are widely distributed in the NKT, which is associated with the assembly of Rodinia continents and the closing of the Proto-Tethys Ocean, respectively [32,33].

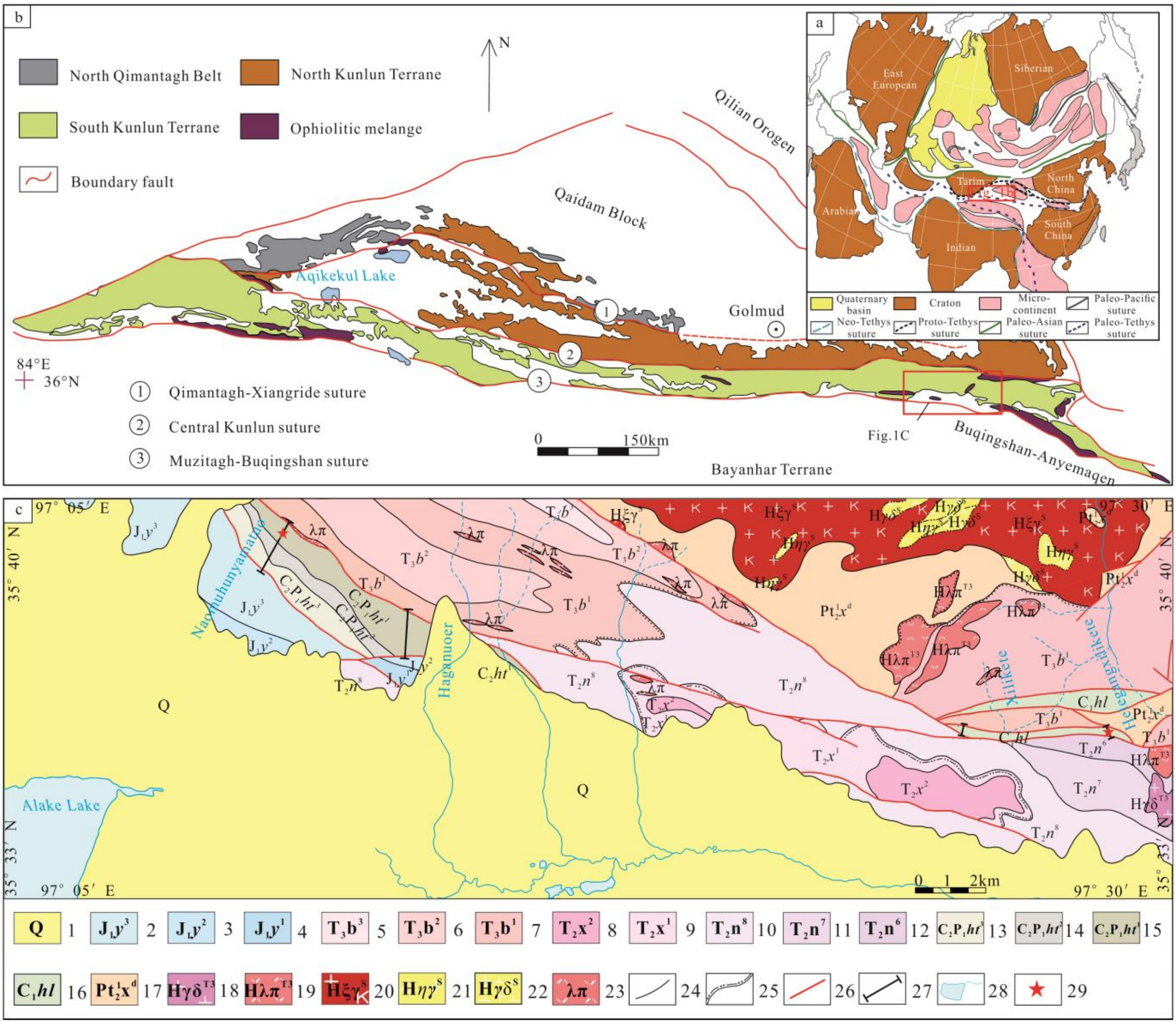

Figure 1. (**a**) Map showing the regional geological background of the EKO (modified from Zhao Guochun et al. [17]); (**b**) Simplified tectonic map showing the tectonic sub-division of EKO (modified from Dong Yunpeng et al. and Li Ruibao et al. [7,9]); (**c**) Geological map for Alake Lake area, eastern EKO. 1—Quaternary; 2—Upper part of Lower Jurassic Yangqu Fm; 3—Middle part of Lower Jurassic Yangqu Fm; 4—Lower part of Lower Jurassic Yangqu Fm; 5—Upper part of Upper Triassic Babaoshan Fm; 6—Middle part of Upper Triassic Babaoshan Fm; 7—Lower part of Upper Triassic Babaoshan Fm; 8—Upper part of Middle Triassic Xilikete Fm; 9—Lower part of Middle Triassic Xilikete Fm; 10—Part 8 of Middle Triassic Naocangjiangou Fm; 11—Part 7 of Middle Triassic Naocangjiangou Fm; 12—Part 6 of Middle Triassic Naocangjiangou Fm; 13—Upper part of Upper Carboniferous to Lower Permian Haoteluowa Fm; 14—Middle part of Upper Carboniferous to Lower Permian Haoteluowa Fm; 15—Lower part of Upper Carboniferous to Lower Permian Haoteluowa Fm; 16—Lower Carboniferous Halaguole Fm; 17—part d of Middle Proterozoic Xiaomiao Fm; 18—Late Triassic biotite granodiorite; 19—Late Triassic rhyolite; 20—Silurian K–feldspar granite; 21—Silurian monzogranite; 22—Silurian granodiorite; 23—rhyolitic dyke; 24—geological boundary; 25—angular unconformity; 26—fault; 27—measured profile location; 28—Lake and river; 29—sample locations for zircon U–Pb age.

The Precambrian metamorphic basement of the SKT is also dominated by the Paleoproterozoic Jinshuikou, Mesoproterozoic Kuhai, and Xiaomiao Groups and the Neoproterozoic

Wanbaogou Group [30]. The Kuhai Group contains paragneisses, amphibolites, and marbles and the Wanbaogou Group is dominated by clastic rocks, limestone, and basaltic–andesitic volcanic rocks [34,35]. The Xiaomiao Group can be sub-divided into four units: quartzite unit, Al-rich gneiss unit, felsic gneiss unit, and quartzite–arkose–quartzite unit [36,37]. In addition, the Neoproterozoic to Early Paleozoic volcanic–sedimentary rocks and Permian to Triassic terrestrial strata occur in the SKT [32].

The study area is geographically near the Alake Lake and located on the southern slope of the eastern SKT (Figure 1c). The Xiaomiao Group, Lower Carboniferous Halaguole, Upper Carboniferous to Lower Permian Haoteluowa, Middle to Lower Permian Maerzheng formations, and Mesozoic siliciclastic rocks are exposed in this area, due to an intrusion by Late Triassic granitoids [20,21,38].

Halaguole and Haoteluowa formations outcrop in the Helegangxilikete–Xilikete and Naomuhunyamatuo–Haganuoer areas in the northeastern part of the Alake Lake, EKO (Figures 1 and 2). The Halaguole Fm is a package of dark gray terrigenous siliciclastic and gray carbonate rocks. The lower part is mainly composed of 30 m to 50 m thick dark gray quartz arenite and bioclastic limestone (Figure 2). The middle part is dominated by 130 m thick dark gray quartz sandstone and calcareous siltstone (Figure 2), whereas the upper dark gray bioclastic limestone and silty mudstone part has a thickness of 88 m. There is typically horizontal and parallel bedding in Halaguole Fm. These rocks are interpreted as being deposited in a shallow marine environment.

The Haoteluowa Fm is a package of gray to dark gray terrigenous clastic and carbonate rocks. The lower part is mainly composed of 720 m thick, thin to medium-bedded gray quartz arenite, and minor bioclastic limestone (Figure 2). The middle part is dominated by 342 m thick medium-bedded gray lithic feldspar sandstone (Figure 2). In comparison, the upper part consists of a package of thin to medium-bedded gray argillaceous siltstone and quartz sandstone, with variable thicknesses between 400 and 450 m from east to west.

Strictly speaking, there are no distinguishable differences in lithological assemblages between these four measured sections. All the sections are dominated by dark gray terrigenous siliciclastic rocks that are interbedded with gray carbonate rocks, with occasional calcareous conglomerate layers occurring in the middle section (Figure 3). This demonstrates that these sections were deposited in a shallow sea environment. In addition, coral and fusulinid fossils (*Dibunophyllum* sp., *Kueichouphyllum* sp., and *Triticites* sp.,) in the limestones also indicate that these sections were deposited in a shallow sea environment [39,40].

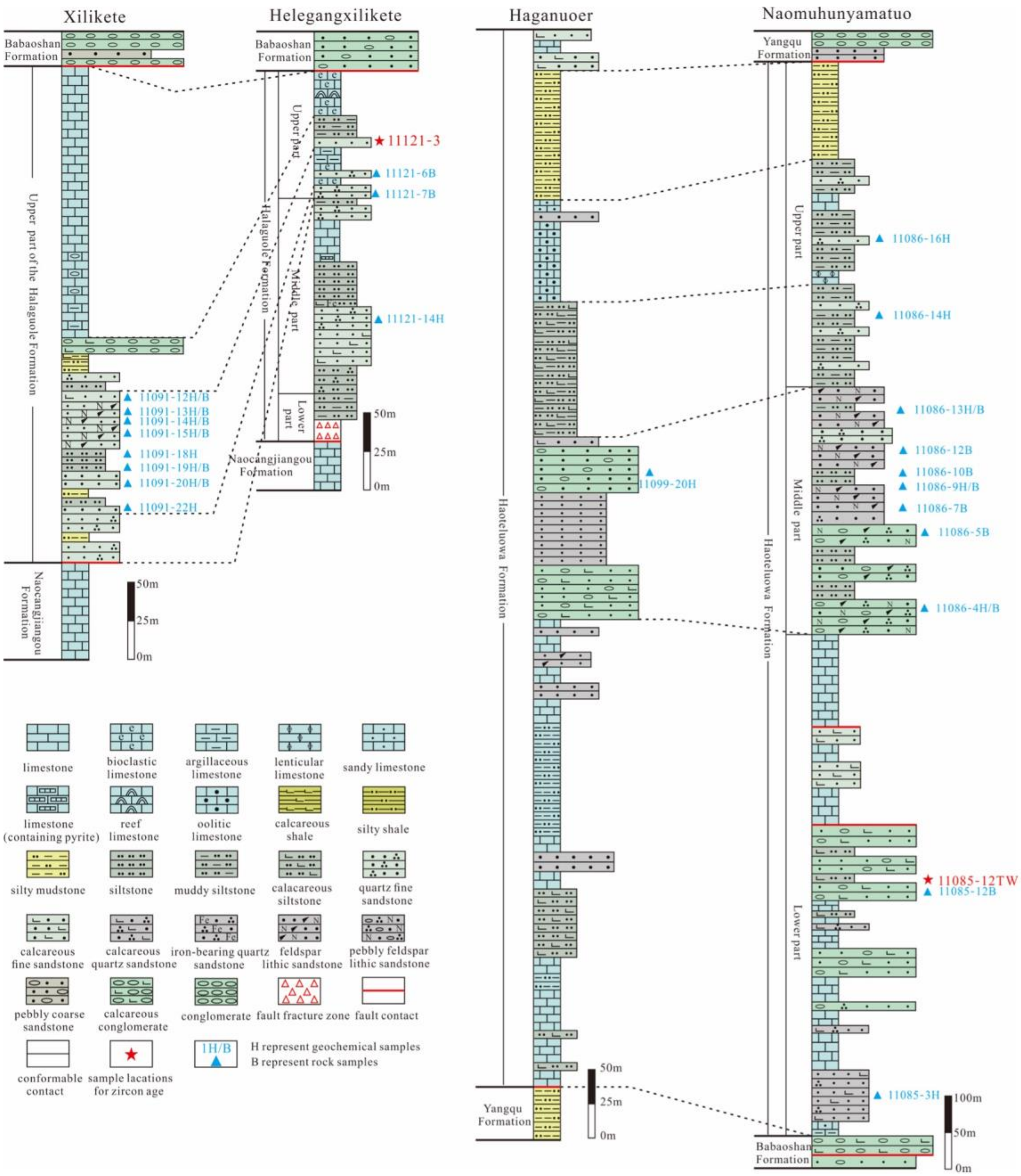

Figure 2. Measured sections of Carboniferous succession in Alake Lake, eastern EKO. Location of sections are shown in Figure 1c.

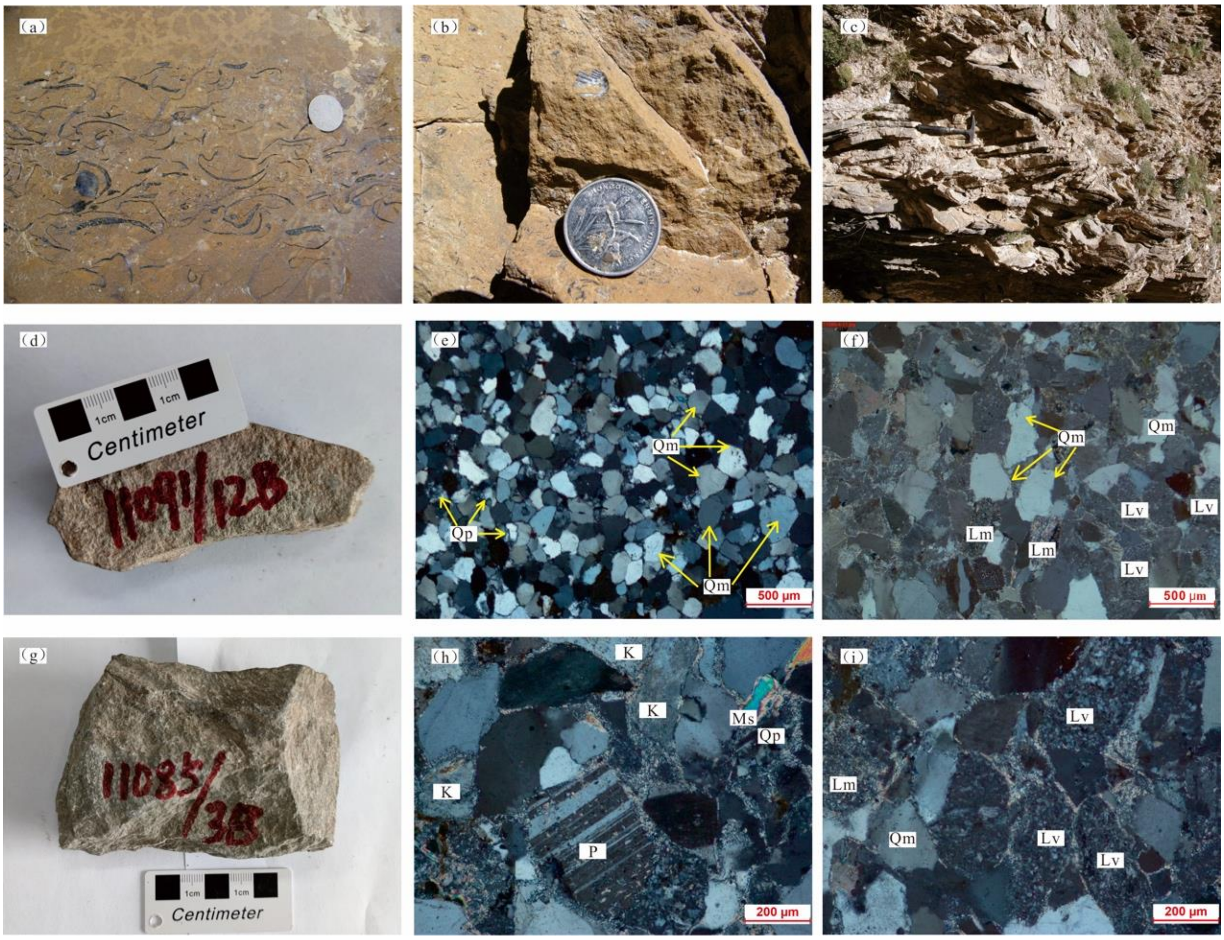

Figure 3. Outcrop, hand specimens, and microscope photographs of the Carboniferous sandstones in the Alake Lake, EKO. (**a**) Lower Carboniferous Halaguole Fm biological shell; (**b**) Lower Carboniferous Halaguole Fm bioclast; (**c**) Lower Carboniferous Halaguole Fm banded limestone; (**d**–**f**) the hand specimens and microscopic photographs of Lower Carboniferous Halaguole Fm fine sandstone; (**g**–**i**) the hand specimens and microscopic photographs of Upper Carboniferous to Lower Permain Haoteluowa Fm siltstone; Mineral abbreviations: Qm—monocrystalline quartz; Qp—polycrystalline quartz; K—K-feldspar; P—plagioclase; Lv—volcanic debris; Lm—metamorphic debris; Ms—muscovite.

3. Analytical Methods

3.1. Whole-Rock Geochemistry

Samples were washed and trimmed, and then crushed and powdered to a size of about 200 mesh (about 0.074 mm) in an agate mill for analysis. The major oxide composition of sandstone samples was analyzed by X-ray fluorescence (XRF; RigkuRIX 2100) spectrometry at the Wuhan Sample Solution Analytical Technology Co., Ltd., Wuhan, China. The analytical precisions were estimated at ca. 5% for major oxides. Sample preparation and other details followed Liu Yongsheng et al. [41].

Trace elements, including rare earth elements, were analyzed by ICP–MS (PE 6100 DRC) at Wuhan Sample Solution Analytical Technology Co., Ltd., Wuhan, China. Pretreatments of the samples were performed as follows. Firstly, powdered samples (50 mg) were dissolved with an HF/HNO_3(1:1) mixture in high-pressure Teflon bombs at 190 °C for 48 h and then evaporated with 3.0 mL HNO_3 after cooling. Then, 3.0 mL 50% (v/v) HNO_3 was added, and the bombs were capped for digestion within an oven at 150 °C for 12 h. Finally, the residue was transferred to a clean PET (polyester) bottle after cooling, and the Rh internal standard was added and then diluted to 80.00 g with deionized water. Elemental standards BHVO–1 (basalt) and AGV–1 (andesite) were used to calibrate elemental concentrations of the measured samples. The precisions of the trace element values were generally better than 2%. Details followed Liu Yongsheng et al. [41].

3.2. Detrital Zircon U–Pb Dating

The zircon separation adopted standard heavy liquid and magnetic methods to produce a concentrate for handpicking. Over 300 grains for each sample were mounted in epoxy, and then polished and gold coated. Cathodoluminescence (CL) images were taken to observe internal textures using a Quanta 650 Scanning Electron Microscope at Xi'an Ruishi Geological Analytical Technology Co., Ltd., Xi'an, China. These pictures, together with transmitted and reflected light images, were used to choose appropriate domains for the U–Pb isotope analyses. Zircon U–Pb analyses were taken by LA–ICP–MS at the Wuhan Sample Solution Analytical Technology Co., Ltd., Wuhan, China. Detailed operating process and equipment conditions can be found in the methodology of Zong Keqing et al. [42]. The laser system consists of a COMPex PRO102 ArF excimer laser (wavelength of 193 nm and maximum energy of 200 MJ) and a Micro Las optical system. Ion signal intensities were acquired using an Agilent 7700e ICP–MS. The spot size and frequency of the laser were set to 35 μm and 42 Hz, respectively. Zircon 91,500 and glass NIST610 were used as external standards for U–Pb dating and trace element calibration, respectively. Excel-based software, ICPMSData Cal, was used to perform off-line selection and integration of background and analyzed signals, time–drift correction, and quantitative calibration for the trace element analysis and U–Pb dating [41].

4. Results

4.1. Petrography

Sandstones from Halaguole and Haoteluowa formations mainly consist of quartz, feldspar, and lithic grains. The abundance of quartz grains vary from 30% to 99%, and the quartz grains are composed of monocrystalline (Qm/Q = 26–97%) and polycrystalline (Qp/Q = 2–9%) grains. Most of the quartz grains are angular–subangular, indicating no long-distance grain transportation. The monocrystalline quartz grains are smooth on the surface, are mostly subhedral, and locally contain small gas–liquid inclusions, indicating a volcanic origin. However, polycrystalline quartz grains mainly consist of quartzite and metamorphosed chert combined with elongated polycrystalline quartz, implying a metamorphic rock source [43]. The feldspar grains are mainly composed of plagioclases displaying polysynthetic twinning, as well as a small amount of potassium feldspar.

Lithic fragments consisted of volcanic, minor metamorphic, and sedimentary rock fragments. The igneous lithic fragments were dominated by volcanic rock fragments with felsic and microlithic textures in all the measured sections. Metamorphic lithic fragments (0–16%), including slate, phyllite, and schist lithic fragments, were characterized by schistose fabrics. Sedimentary lithic fragments (0–16%) included limestone and mudstone lithic fragments, which accounted for a small proportion of the clastic components.

4.2. Major and Trace Elements

Sixteen sandstone samples from Halaguole and Haoteluowa formations were selected for a whole-rock geochemical analysis (Figure 2). Their major and trace elements data are listed in Supplementary Materials Table S1.

The sandstones in the Halaguole Fm have a wide compositional range as follows: SiO_2 (65.78–77.41 wt%), Al_2O_3 (11.27–15.34 wt%), MgO (0.84–1.69 wt%), CaO (0.90–7.82 wt%), Na_2O (0.36–2.67 wt%), K_2O (1.54–3.84 wt%). The sandstones in the Haoteluowa Fm show a similar compositional range: SiO_2 (64.42–79.18 wt%), Al_2O_3 (11.27–19.39 wt%), MgO (0.29–3.34 wt%), CaO (0.25–7.82 wt%), Na_2O (0.28–3.64 wt%), K_2O (1.54–3.84 wt%). In comparison with international standards (e.g., post-Archean Australian shale (PAAS), North American shale composite (NASC), and upper continental crust (UCC), these sandstones are characterized by relatively higher SiO_2 and lower Al_2O_3, $Fe_2O_3{}^T$, MgO, and K_2O contents.

All the sandstone samples show flat rare earth element (REE) patterns (Figure 4a) with a slight enrichment in light REEs (LREEs) and relative depletion in heavy REEs (HREEs) (La_N/Yb_N = 1.49–10.38 and 6.95–9.66; Gd_N/Yb_N = 0.74–1.76 and 1.25–1.50). Additionally, most of the sandstones show distinctly negative Eu anomalies (Eu/Eu* = 0.06–0.75 and 0.36–0.74). The Cs, Th, Ta, and Li contents were higher than the average upper continental crust (UCC) calculated by Taylor and McLennan [44], whereas Sr and Ni were lower than the UCC values (Figure 4b).

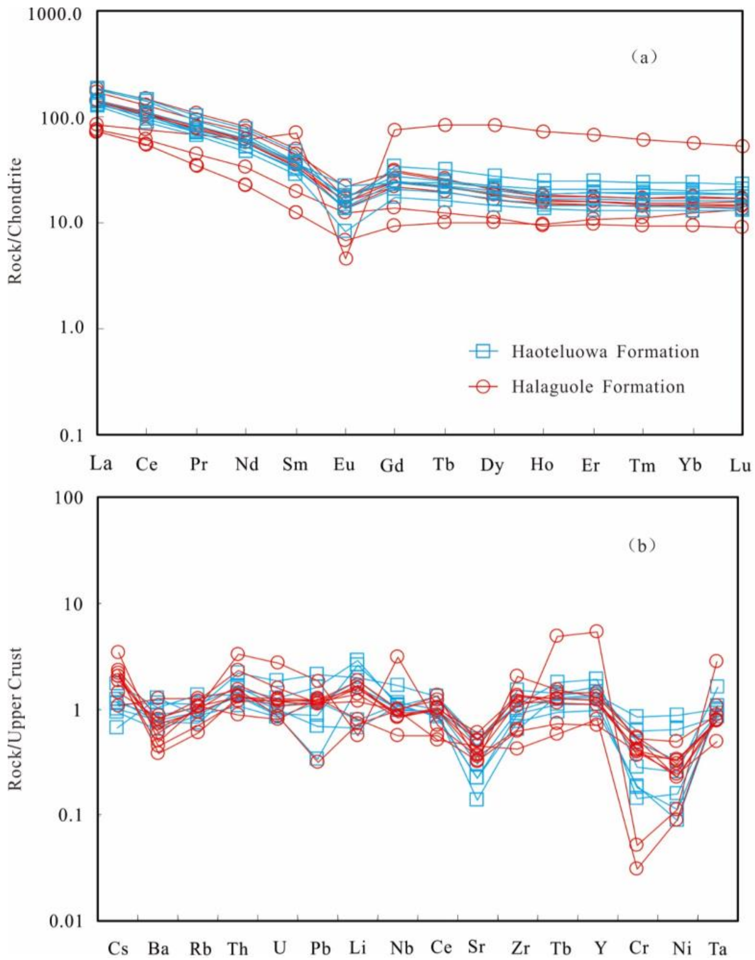

Figure 4. (**a**) Chondrite-normalized REE patterns (Chondrite data from Sun and McDonough [44]), and (**b**) upper crust-normalized trace element spider pattern of the sandstones from Alake Lake, EKO (upper crust data from Taylor and McLennan [45]).

4.3. Detrital Zircon U–Pb Ages

4.3.1. Detrital Zircon Morphology

These detrital zircons are 70–140 μm long with aspect ratios of 1:1 to 3:1, and are dominated by angular to subangular morphology, which likely indicates short distance transportation (Figure 5). In the cathodoluminescence (CL) images, most detrital zircons show low luminescence, but the presence of oscillatory zoning and their high Th/U ratios suggest that most of them have an igneous origin (Figure 5a,b) (Th/U > 0.1, clear oscillatory zoning), and only a few grains may have a metamorphic origin (Th/U < 0.1, no oscillatory zoning) [46].

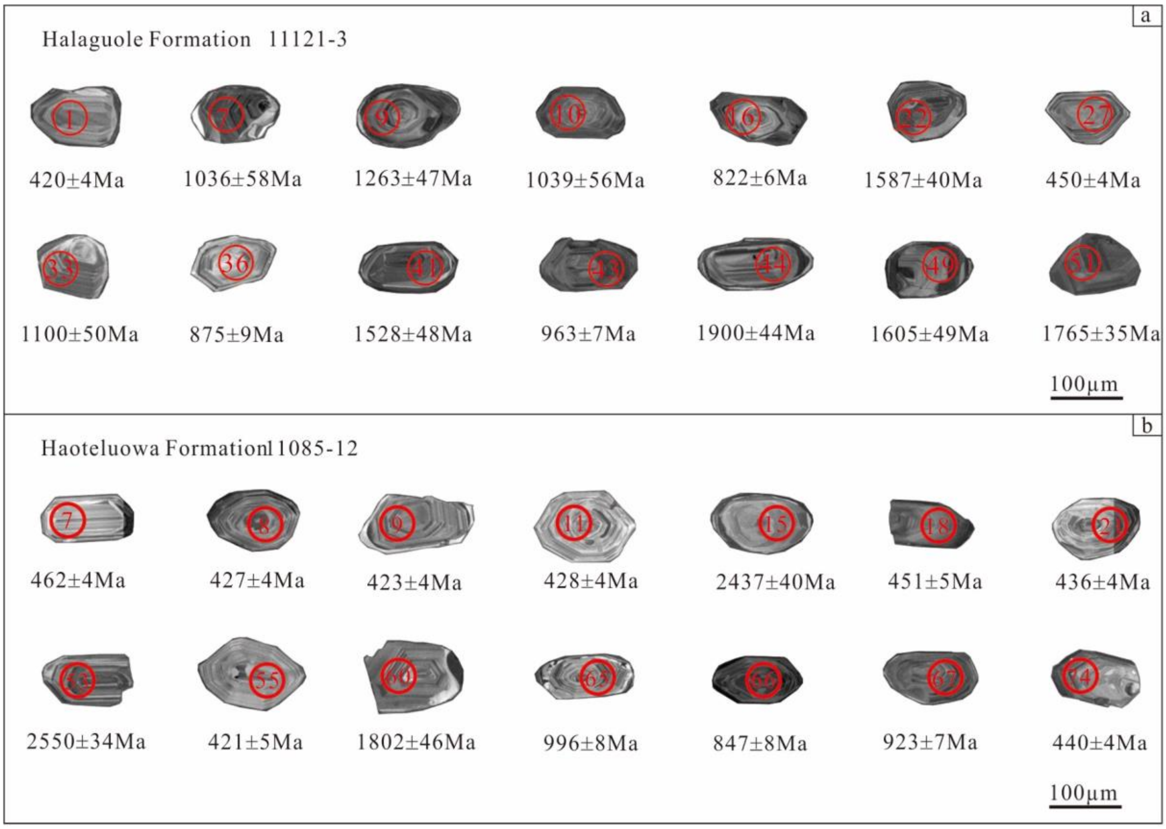

Figure 5. Typical CL images of detrital zircons from the Halaguole and Haoteluowa formations, EKO. The circles on zircons show the locations of U–Pb dating.

4.3.2. Detrital Zircon U–Pb Ages

A total of 159 detrital zircons from two sandstone samples of Halaguole and Haoteluowa formations were analyzed. Detrital zircon U–Pb ages are shown in Supplementary Materials Table S2. Zircons older than 1000 Ma are discussed based on $^{207}Pb/^{206}Pb$ ages [47], while younger zircons are based on $^{206}Pb/^{238}U$ ages [48,49].

Eighty analyses were obtained from the Halaguole Fm (sample no. 11121–3). All eighty analyses from the sample 11121–3 (Halaguole Fm) plot along the concordia line show a complicated age spectrum (Figure 6b). Early Paleozoic zircons have a range from 405 to 475 Ma, with a dominant age peak at 440 Ma. Twenty-three Neoproterozoic zircons cover an age range between 781 and 999 Ma, with an age peak at 983 Ma. Twenty-three zircons have Mesoproterozoic ages of 1010 to 1529 Ma, with an age peak at 1175 Ma and two minor age peaks at 1136 Ma and 1524 Ma. Paleoproterozoic to Archean zircons have a range from 1647 to 2997 Ma, with a main peak age at 1902 Ma and two minor peak ages at 1814 and 2420 Ma.

Seventy-nine analyses were obtained from the Haoteluowa Fm (sample no. 11085–12), of which seventy-seven concordant ages were obtained (Figure 6c,d). Early Paleozoic zircons have a range from 421 to 503 Ma, with a dominant age peak at 440 Ma. Fourteen Neoproterozoic zircons cover an age range between 792 and 996 Ma, with an age peak at 988 Ma. Twenty-three zircons have Mesoproterozoic ages of 1002 to 1191 Ma, with an age peak at 1189 Ma. Paleoproterozoic to Archean zircons have a range from 1610 to 2652 Ma, with a main peak age at 2564 Ma and two minor peak ages at 1672 and 2130 Ma.

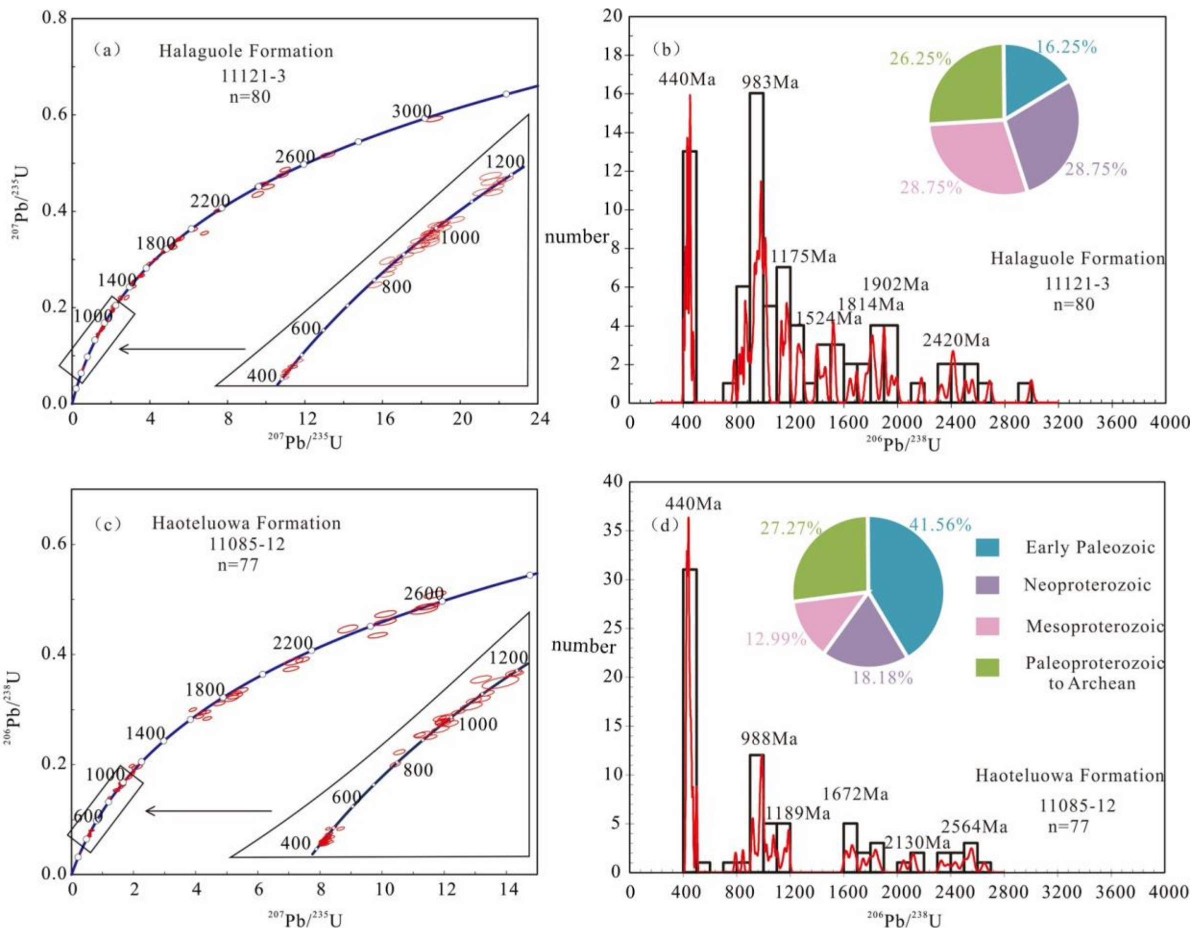

Figure 6. U–Pb concordia diagrams and histogram for detrital zircons from Carboniferous sandstones in Alake Lake, EKO. (**a**,**c**) Concordia diagram of detrital zircons from the Halaguole and Haoteluowa formations; (**b**,**d**) Histogram of detrital zircons from the Halaguole and Haoteluowa formations.

5. Discussion

5.1. Provenance Characteristics

The Chemical Index of Alteration (CIA) is a common parameter used to reveal the degree of source area chemical weathering and source composition of clastic rocks [50–52]. The calculation formula for the CIA is as follows: CIA = $[Al_2O_3/(Al_2O_3 + CaO^* + Na_2O + K_2O)] \times 100$ (molar proportions). As there is no information on CO_2 with which to adjust for the Ca in carbonates, CaO* stands for the CaO content in the silicate fraction and is determined by comparing the Na_2O content. If CaO $\leq$ Na_2O, it directly took the value of CaO as that of CaO*; if not, we assumed that the CaO* concentration equaled that of Na_2O [53]. The CIA values of the Halaguole Fm sandstone (49.48–74.20; averaging 57.83) and the Haoteluowa Fm sandstone (55.90–78.69; averaging 64.66) are close to those of the NASC (CIA = 58; [54]) and Archean graywacke (CIA = 58; [55]) but lower than those of the PAAS (CIA = 70; [45,56]) and cratonic sandstone and shales (CIA = 69–77; [55]). The majority of the samples plot within the weak chemical weathering field on the $Al_2O_3 - (CaO^* + Na_2O) - K_2O$ (A–CN–K) triangular diagram (Figure 7) [50,51,57]. All these features suggest that the Halaguole and Haoteluowa formation sandstones experienced a low degree of chemical modification and short-distance transportation.

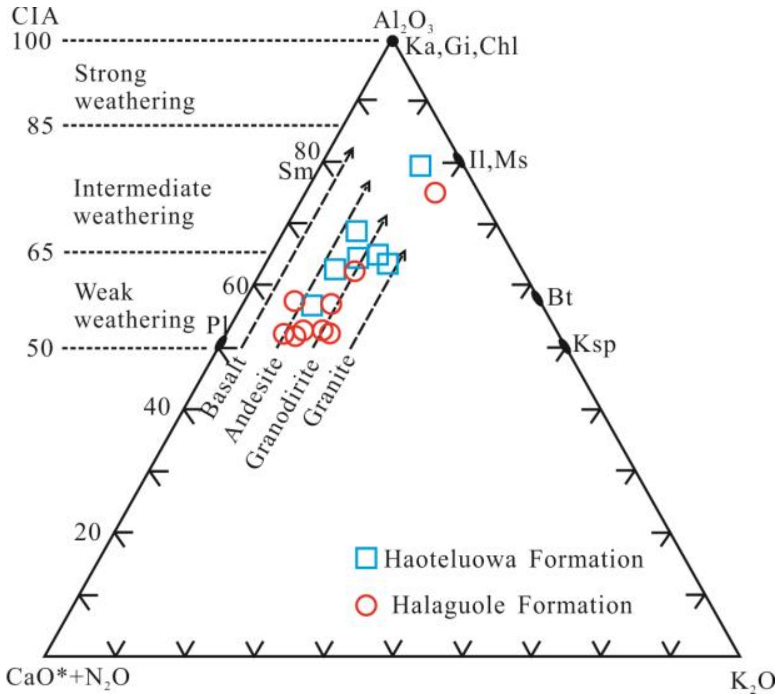

Figure 7. A–CN–K triangular diagram of sandstones for the Carboniferous sandstones in Alake Lake, EKO (after Nesbitt and Young [50,57]; Fedo et al. [51]). Data for tonalite (To), granodiorite (Gd), granite (Gr), and average post-Archean upper crust are from Condie [55]. Abbreviations for minerals: Pl—plagioclase; K–sp—potassic feldspar; Ka—kaolinite; Chl—chlorite; Gi—gibbsite; Sm—smectite; IL—illite; Ms—muscovite.

Trace element compositions are mainly controlled by source area components and the tectonic environment [45]. As an effective indicator of provenance components, the Al_2O_3/TiO_2 ratio of sandstones and mudstones is fundamentally identical to those of their source [58]. Generally, detrital materials from felsic rocks have Al_2O_3/TiO_2 ratios ranging from 21 to 70 [58–60]. The average Al_2O_3/TiO_2 ratios of the Halaguole and Haoteluowa formation sandstones are 39 and 46, respectively, implying that they are mainly derived from felsic sources. Moreover, the relatively low (0.56–2.88) La/Th ratios and Hf contents of 3.01–10.05 ppm (Figure 8a) also indicate a main felsic magmatic provenance with minor or little influence from old sedimentary and intermediate igneous components [61] (Figure 8a). This is also supported by their high Rb and K_2O contents (Figure 8b), and they all plot within the intermediate acid region in the Rb vs. K_2O and F1 vs. F2 diagrams (Figure 8c).

In addition, zircon trace elements can also serve as a basis for provenance studies and reflect the host rock type [62]. Almost all (~98.7%) of the detrital zircon grains from these samples have Th/U ratios of >0.1, suggesting a main origin of igneous rocks [46]. The Y and U concentrations, as well as their relationship, were used to discriminate between the different rock types. Most Early Paleozoic to Neoproterozoic detrital zircons have high Y and U contents and Y/Sm ratios, indicative of the derivation of a granitic composition for their provenance [62–64] (Supplementary Materials Figure S1a–d). In addition, the characteristics of the trace element compositions also suggest similar granitic sources; the results shown in Supplementary Materials Figure S1e were calculated by the previously proposed classification and regression tree method [62] (Supplementary Materials Figure S1).

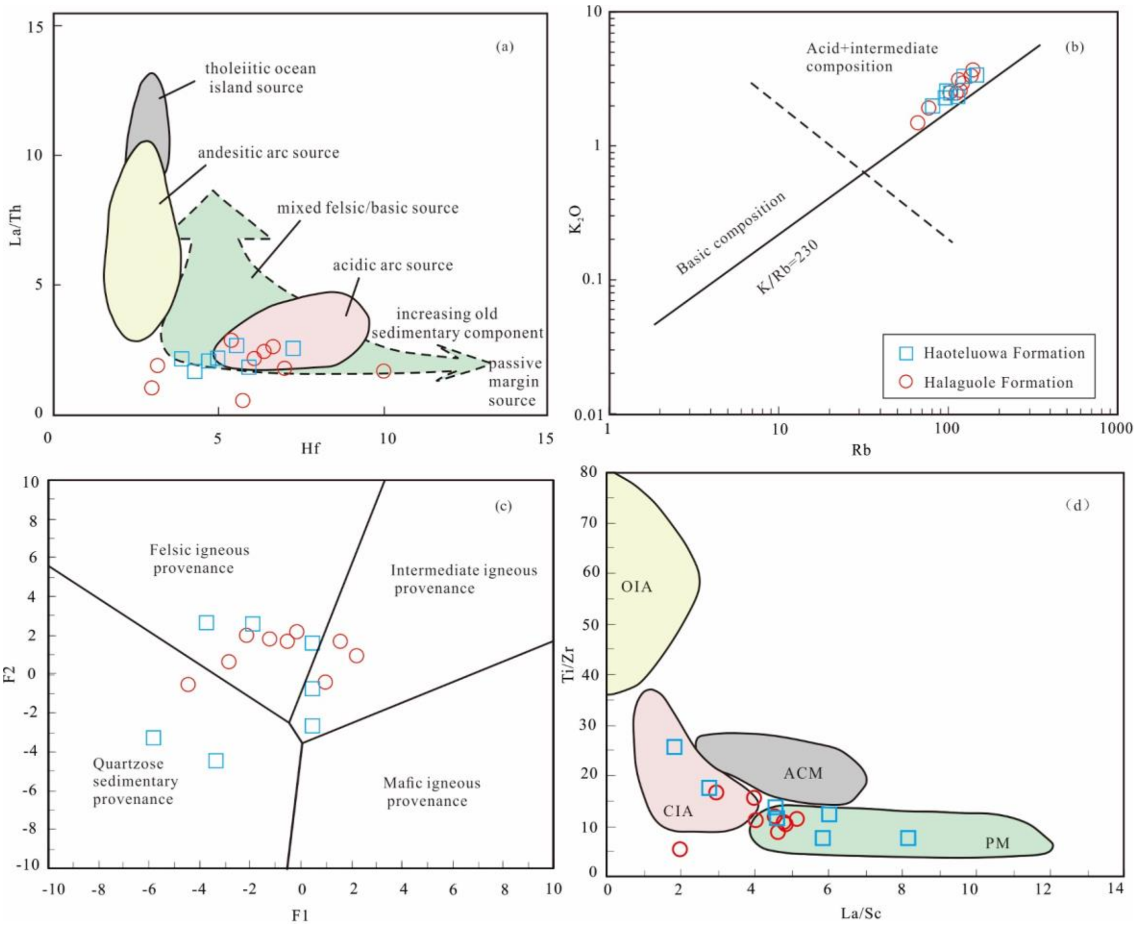

Figure 8. Geochemical diagrams showing variations in source composition and tectonic setting discrimination for the Carboniferous sandstones in Alake Lake, EKO. (**a**) La/Th–Hf diagram (after Floyd et al. [65]); (**b**) K_2O–Rb diagram (after Floyd et al. [65]); (**c**) F1–F2 diagram (after Roser et al. [66]); (**d**) Ti/Zr–La/Sc (after Bhatia and Crook [67]). F1 = $-1.773TiO_2 + 0.607Al_2O_3 + 0.76\ Fe_2O_3{}^T - 1.5MgO + 0.616CaO + 0.509Na_2O - 1.224\ K_2O - 9.09$. F2 = $0.445TiO_2 + 0.07Al_2O_3 - 0.25\ Fe_2O_3{}^T - 1.142MgO + 0.438CaO + 1.457Na_2O + 1.426\ K_2O - 6.861K_2O/Al_2O_3 - 3.890$.

All the measured sections' samples had 100 × TiO_2/Fe_2O_3(T) and 100 × TiO_2/Al_2O_3 values similar to the average values for felsic volcanic rocks, such as granite. This implies that they may be mostly from granitoid sources. The Al_2O_3/TiO_2, $(La/Yb)_N$, Eu/Eu*, La/Sc, Th/Sc, La/Th, Zr/Sc, and Th/Sc values further underline a predominantly felsic (granitic) source for the detritus (Supplementary Materials Table S3).

Our detrital zircon U–Pb ages for the sandstone samples show a broad age span from the Archean to the Early Paleozoic era (Figure 6b,d). Their age spectra are typically characterized by four distinct age populations at 405–503 Ma (peak at ~437 Ma), 781–999 Ma (peak at ~984 Ma), 1002–1529 Ma (peak at ~1184 Ma), and 1610–2997 Ma (peak at ~2510 Ma) (Figure 9), which show similar tectono–thermal events with the North Qimatag Belt (NQB), North Kunlun Terrane (NKT), and South Kunlun Terrane (SKT) (Figure 9). Furthermore, detrital zircon ages from both Halaguole and Haoteluowa formations have peaks at ca. 437 Ma and ca. 984 Ma, which is an important signature of the NQB, NKT, and SKT [68]. In summary, sandstone geochemistry and detrital zircon U–Pb ages indicate that the NQB, NKT, and SKT should probably be the main sedimentary provenance of Halaguole and Haoteluowa formations.

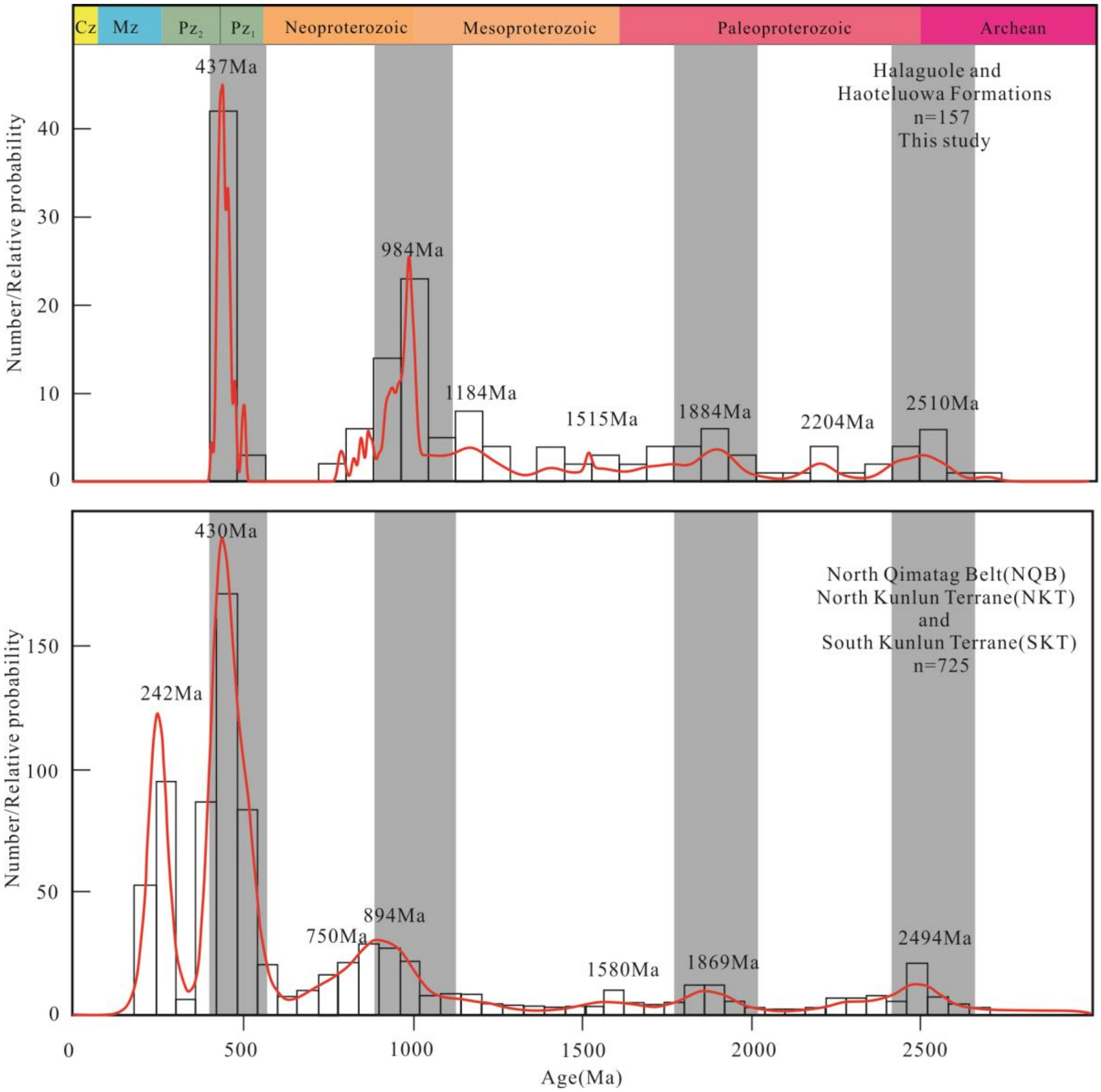

Figure 9. Comparison of detrital zircon ages from the sedimentary rocks in this study and those from the counterparts in the East Kunlun Orogen [68]. The gray boxes represent the areas where the age peaks of zircons for clastic rocks of East Kunlun Orogen.

5.2. Tectonic Setting

Previous researchers have reconstructed the general tectonic framework and evolution history of the EKO during Late Paleozoic to the Mesozoic. However, some debate continues regarding the Carboniferous tectonic background in EKO. There are two diametrically contrasting tectonic models for Carboniferous Ocean–continent framework, namely, a subduction zone model [7,8,19] and a passive continental margin setting [10,20–27,69].

We argued that the Carboniferous sedimentary rocks were deposited in a passive continental margin and there was no subduction of oceanic crust during Carboniferous to Early Permian (ca. 358–272 Ma). This conclusion is supported by the following evidence: (1) the Carboniferous sedimentary rocks mainly consist of a package of shallow marine facies terrigenous clastic rocks and platform facies carbonate rocks, which is a typical sedimentary succession formed in a passive continental margin [21,23]; (2) Lower Carboniferous Halaguole and Upper Carboniferous to Lower Permian Haoteluowa formations have comparatively high composition maturity and structure maturity (Supplementary Materials Table S4), and it is comparable to the passive continental margin of the southern Yangtze Block [70]; (3) the Carboniferous to Early Middle Permian subduction-related island arc magmatic rocks have not been discovered in the EKO, which contradict with the active continental setting; (4) most sandstone samples from Halaguole and Haoteluowa formations are plotted in the passive continental margin field (Figure 8d), which implies a passive continental margin setting for Halaguole and Haoteluowa formations; (5) Generally, the youngest detrital zircon ages in extensional basins are often tens or even hundreds of millions of years older than their depositional ages [71]. The youngest detrital zircon age is 440 Ma, which is much older than their depositional age of Carboniferous. In addition, the detrital zircon age distribution patterns imply that Halaguole and Haoteluowa formations were deposited in an extensional setting [71] (Figure 10).

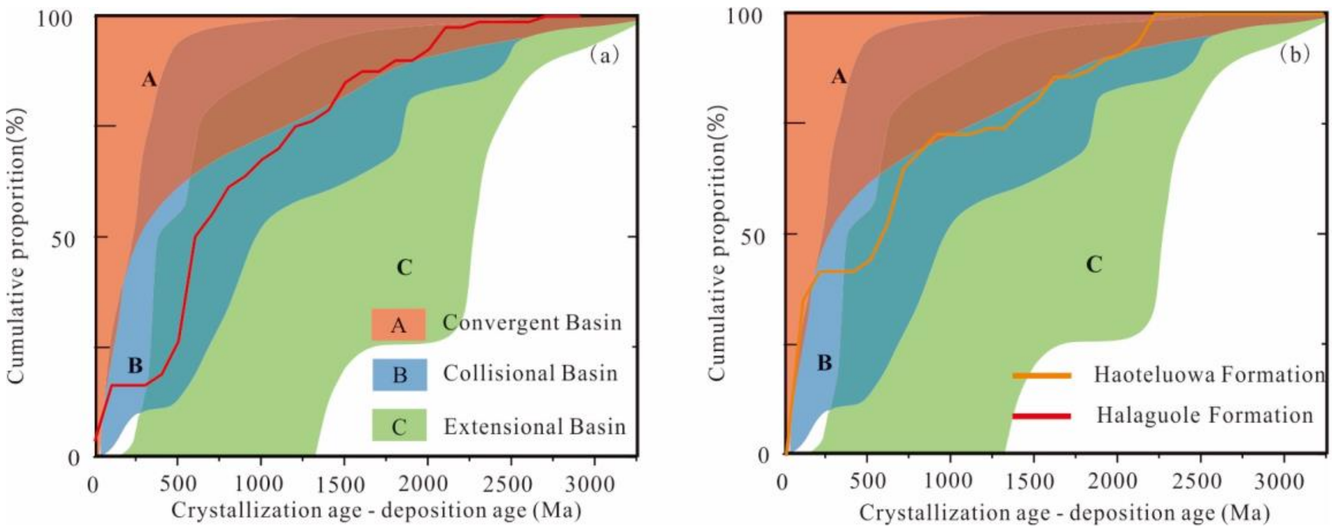

Figure 10. Cumulative probability curve of the difference between the crystalline age and sedimentary age of detrital zircons from the Carboniferous sandstones in the Alake Lake area (after Cawood et al. [71]). (**a**) the crystalline age and sedimentary age of Halaguole formations, (**b**) the crystalline age and sedimentary age of Haoteluowa formations.

Thus, we suggest that Halaguole and Haoteluowa formations were likely deposited in a passive continental margin basin. This conclusion also implies that the Paleo-Tethys Ocean did not begin to subduct northward and there was no oceanic subduction zone in the south EKO during Carboniferous to Early Permian times.

Regionally, the initial opening of the Paleo-Tethyan Ocean may have occurred before the Early Carboniferous time evidenced by earlier oceanic relicts, such as the Buqingshan accretionary complex, containing Early Carboniferous mantle peridotites, MORBs, and OIBs [10,72–74]. From a global perspective, a number of oceans emerged across this region, which is today represented by the Buqingshan, Jinsha, and Central Qiangtang oceans in the Tibet–Qinghai Plateau [17,75–77]. These oceans, which formed a complex ocean–continent combination throughout portions of what is now Asia, were all branches of the Paleo-Tethys Ocean region (Figure 11). Our work further supports the idea that the initial subduction of the Paleo-Tethys Ocean did not occur during the Carboniferous to Early Permian.

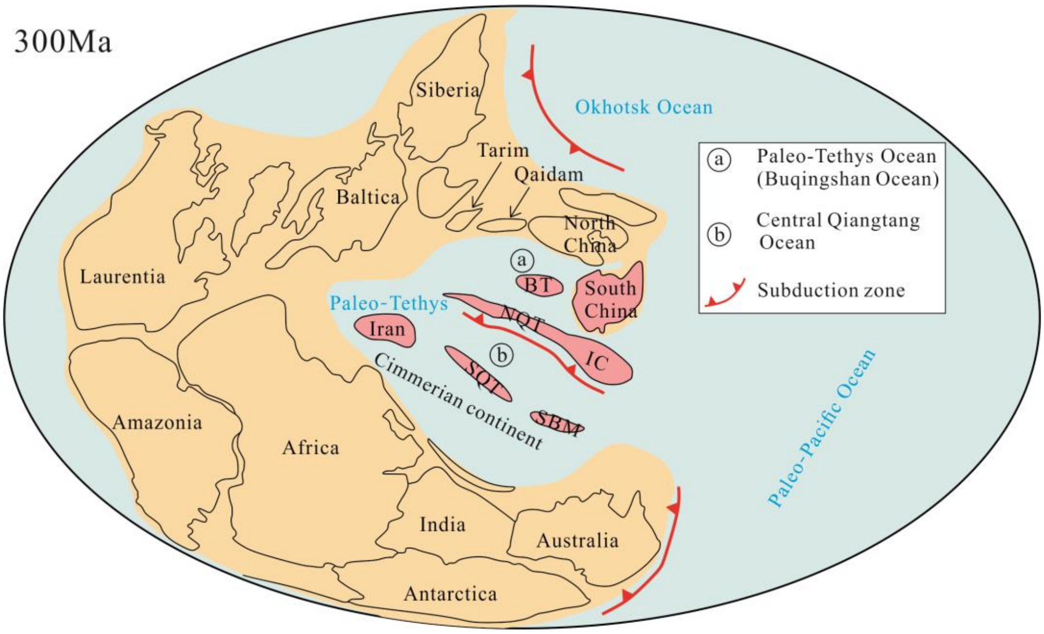

Figure 11. Reconstruction of East Asian blocks showing the spreading of Northern Paleo-Tethys Ocean (Buqingshan Ocean) (modified from [10,17,78–82]. SQT—South Qiangtang Terrane; NQT—North Qiangtang Terrane; BT—Bayan Har terrane; SBM—Sibumasu Terrane; IC—Indochina Terrane.

6. Conclusions

1. Lower Carboniferous Halaguole and Upper Carboniferous–Lower Permian Haoteluowa formations mainly consist of a package of shallow marine facies siliciclastic rocks and platform facies carbonate rocks.
2. A geochemical composition indicates that sandstones from Halaguole and Haoteluowa formations experienced a low degree of chemical weathering and their source rocks are mainly acidic igneous rocks with a minor contribution of old sedimentary components.
3. The detrital zircon U–Pb age spectrum of these sandstone samples is dominated by age peaks at ~405–503 Ma and ~781–999 Ma, with subordinate age peaks at ~1610–2997 Ma and ~1002–1529 Ma, which show similar tectono–thermal events with the North Qimatag Belt (NQB), North Kunlun Terrane (NKT), and South Kunlun Terrane (SKT).
4. The Halaguole and Haoteluowa formations were likely deposited in a stable passive continental margin environment, not a subduction zone setting.

Supplementary Materials: The following supporting information can be downloaded at: https://www.mdpi.com/article/10.3390/min13030312/s1, Table S1: Major element (%) and trace and rare earth element (×10–6) analysis data of Carboniferous sandstones from the Alake Lake area; Table S2: LA–ICP–MS zircon U–Pb age test results of Carboniferous System clastic rocks in Alake Lake area; Table S3: Geochemical comparison of four measured sections of the Carboniferous in Alake Lake area; Table S4: Statistics of sandstone clastic components of the Carboniferous in Alake Lake area; Figure S1: Trace element characteristics of the detrital zircons from the Halaguole and Haoteluowa formations. References [46,62] are cited in the Supplementary Materials.

Author Contributions: Conceptualization, X.W. and X.P.; methodology, Z.L.; software, X.W.; formal analysis, X.P. and R.L.; investigation, X.W., X.P., R.L., C.L., L.P., Z.L. and Y.C.; resources, Z.L.; data curation, X.W., X.P. and C.L.; writing—original draft preparation, X.W. and X.P.; writing—review and editing, X.P., R.L., Y.C. and M.W.; supervision, X.P.; funding acquisition, X.P., Z.L. and R.L. All authors have read and agreed to the published version of the manuscript.

Funding: This research was funded by the National Nature Sciences Foundation of China (grant numbers 42172236, 41802234, 41872235, 41502191), Natural Science Basic Research Plan in Shaanxi

Province of China (grant numbers 2019JM-312, 2019JQ-090, 2019JQ-209, 2020JM-229), the Fundamental Research Funds for the Central Universities (grant numbers 300102270202, 300103183081, 300103120009, 300104282717, 300102279204, 201810710233), the Commonweal Geological Survey, the Aluminum Corporation of China and the Land-Research Department of Qinghai Province (grant number 200801), and the Youth Innovation Team of Shaanxi Universities.

Data Availability Statement: The original contributions presented in the study are included in the article/Supplementary Materials.

Acknowledgments: We are grateful to Hai Zhou, Shaowei Zhao, Jie Zhao, Lili Xu, and Mao Wang for their insightful and constructive comments both in science and English, which substantially improved the manuscript. Special thanks are extended to the chief editor and the two anonymous reviewers for their constructive reviews which have greatly improved our manuscript.

Conflicts of Interest: The authors declare no conflict of interest.

References

1. Fonneland, H.C.; Trond, L.; Martinsen, O.J.; Pedersen, R.B.; Košler, J. Detrital zircon ages: A key to understanding the deposition of deep marine sandstones in the Norwegian Sea. *Sediment. Geol.* **2004**, *164*, 147–159. [CrossRef]
2. Dong, Y.P.; Liu, X.M.; Neubauer, F.; Zhang, G.W.; Tao, N.; Zhang, Y.G.; Zhang, X.N.; Li, W. Timing of Paleozoic amalgamation between the North China and South China Blocks: Evidence from detrital zircon U–Pb ages. *Tectonophysics* **2013**, *586*, 173–191. [CrossRef]
3. Veevers, J.J.; Saeed, A. Age and composition of Antarctic sub-glacial bedrock reflected by detrital zircons, erratics, and recycled microfossils in the Ellsworth Land–Antarctic Peninsula–Weddell Sea–Dronning Maud Land sector (240° E–0°–015° E). *Gondwana Res.* **2013**, *23*, 296–332. [CrossRef]
4. Bauluz, B.; Mayayo, M.J.; Fernandez Nieto, C.; Lopez, J.M.G. Geochemistry of Precambrian and Paleozoic siliciclastic rocks from the Iberian Range (NE Spain): Implications for source-area weathering, sorting, provenance, and tectonic setting. *Chem. Geol.* **2000**, *168*, 135–150. [CrossRef]
5. Yan, Z.; Wang, Z.Q.; Wang, T.; Yan, Q.R.; Xiao, W.J.; Li, J.L. Provenance and Tectonic Setting of Clastic Deposits in the Devonian Xicheng Basin, Qinling Orogen, Central China. *J. Sediment. Res.* **2006**, *76*, 557–574. [CrossRef]
6. Fathy, D.; Abart, R.; Wagreich, M.; Gier, S.; Ahmed, M.S.; Sami, M. Late Campanian Climatic-Continental Weathering Assessment and Its Influence on Source Rocks Deposition in Southern Tethys, Egypt. *Minerals* **2023**, *13*, 160. [CrossRef]
7. Dong, Y.P.; He, D.F.; Sun, S.S.; Liu, X.M.; Zhou, X.H.; Zhang, F.F.; Yang, Z.; Cheng, B.; Zhao, G.C.; Li, J.H. Subduction and Accretionary Tectonics of the East Kunlun Orogen, Western Segment of the Central China Orogenic System. *Earth Sci. Rev.* **2018**, *186*, 231–261. [CrossRef]
8. Dong, Y.P.; Sun, S.S.; Santosh, M.; Zhao, J.; Sun, J.P.; He, D.F.; Shi, X.H.; Hui, B.; Cheng, C.; Zhang, G.W. Central China Orogenic Belt and Amalgamation of East Asian Continents. *Gondwana Res.* **2021**, *100*, 131–194. [CrossRef]
9. Li, R.B.; Pei, X.Z.; Wei, B.; Li, Z.C.; Pei, L.; Chen, G.C.; Chen, Y.X.; Liu, C.J. Middle Cambrian–Early Ordovician ophiolites in the central fault of the East Kunlun Orogen: Implications for an epicontinental setting related to Proto–Tethyan Ocean subduction. *Gondwana Res.* **2021**, *94*, 243–258. [CrossRef]
10. Li, R.B.; Pei, X.Z.; Li, Z.C.; Pei, L.; Chen, G.C.; Liu, Z.Q.; Chen, Y.X.; Liu, C.J.; Wang, M.; Zhang, M. Paleo–Tethyan Ocean Evolution and Indosinian Orogenesis in the East Kunlun Orogen, Northern Tibetan Plateau. *Minerals* **2022**, *12*, 1590. [CrossRef]
11. Yang, J.S.; Robison, P.T.; Jiang, C.F.; Xu, Z.Q. Ophiolites of the Kunlun Mountains, China and their tectonic implications. *Tectonophysics* **1996**, *258*, 215–231. [CrossRef]
12. Yin, A.; Harrison, T.M. Geologic evolution of the Himalayan-Tibetan orogeny. *Annu. Rev. Earth Planet. Sci.* **2000**, *28*, 211–280. [CrossRef]
13. Zhang, G.W.; Dong, Y.P.; Lai, S.C.; Guo, A.L.; Meng, Q.R.; Liu, S.F.; Cheng, S.Y.; Yao, A.P.; Zhang, Z.Q.; Pei, X.Z.; et al. Mianlue Tectonic Zone and Mianlue Suture Zone on Southern Margin of Qinling–Dabie Orogenic Belt. *Sci. China Ser. D* **2003**, *33*, 1121–1135.
14. Xu, Z.Q.; Yang, J.S.; Li, W.C.; Li, Q.H.; Cai, Z.H.; Yan, Z.; Ma, C.Q. Paleo-Tethys system and accretionary orogen in the TibetPlateau. *Acta Petrol. Sin.* **2013**, *29*, 1847–1860.
15. Meng, F.C.; Cui, M.H.; Jia, L.H.; Ren, Y.H.; Feng, H.B. Paleozoic continental collision of the East Kunlun orogen: Evidence from protoliths of the eclogites. *Acta Petrol. Sin.* **2015**, *31*, 3581–3594.
16. Li, S.Z.; Zhao, S.J.; Yu, S.; Cao, H.H.; Li, X.Y.; Liu, X.; Guo, X.Y.; Xiao, W.J.; Lai, S.C.; Yan, Z.; et al. Proto–Tehtys Ocean in East Asia (II): Affinity and assmbly of Early Paleozoic micro–continental blocks. *Acta Petrol. Sin.* **2016**, *32*, 2628–2644.
17. Zhao, G.C.; Wang, Y.J.; Huang, B.C.; Dong, Y.P.; Li, S.Z.; Zhang, G.W.; Yu, S. Geological Reconstructions of the East Asian Blocks: From the breakup of Rodinia to the Assembly of Pangea. *Earth Sci. Rev.* **2018**, *186*, 262–286. [CrossRef]
18. Li, R.B.; Pei, X.Z.; Li, Z.C.; Daniel, P.; Su, Z.G.; Pei, L.; Chen, G.C.; Chen, Y.X.; Liu, C.J. Late Silurian to Early Devonian volcanics in East Kunlun Orogen, northern Tibet Plateau: Record of post-collisional magmatism related to the Proto-Tethyan Ocean evolution. *J. Geodyn.* **2020**, *140*, 101780. [CrossRef]

19. Yue, Y.G.; Dong, Y.P.; Sun, S.S.; He, D.F.; Hui, B.; Ren, X.; Zhang, B.; He, W.D. Mafic-ultramafic rocks in the Buqingshan Complex of the East Kunlun Orogen, northern Tibetan Plateau: Remnants of the Paleo-Tethys Ocean. *Int. Geol. Rev.* **2022**, *64*, 3149–3170. [CrossRef]
20. Li, R.B.; Pei, X.Z.; Li, Z.C.; Liu, Z.Q.; Chen, G.C.; Chen, Y.X.; Wei, F.H.; Gao, J.M.; Liu, C.J.; Pei, L. Geological characteristics of Late Paleozoic-Mesozoic unconformities and their response to some significant tectonic events in eastern part of Eastern Kunlun. *Earth Sci. Front.* **2012**, *19*, 244–254.
21. Li, R.B. Research on the Late Paleozoic–Early Mesozoic Orogeny in East Kunlun Orogen. PH.D. Thesis, Chang'an University, Xi'an, China, 2012.
22. Li, R.B.; Pei, X.Z.; Pei, L.; Li, Z.C.; Chen, G.C.; Chen, Y.X.; Liu, C.J.; Wang, M. The Early Triassic Andean-type Halagatu granitoids pluton in the East Kunlun orogen, northern Tibet Plateau: Response to the northward subduction of the Paleo-Tethys Ocean. *Gondwana Res.* **2018**, *62*, 212–226. [CrossRef]
23. Pei, X.Z.; Hu, N.; Liu, C.J.; Li, R.B.; Li, Z.C.; Chen, Y.X.; Pei, L.; Liu, Z.Q.; Chen, G.C.; Yang, J. Detrital Composition, Geochemical Characteristics and Provenance Analysis for the Maerzheng Formation Sandstone in Gerizhuotuo Area, Southern Margin of East Kunlun Region. *Geol. Rev.* **2015**, *61*, 307–323.
24. Pei, L.; Li, R.B.; Pei, X.Z.; Liu, J.L.; Li, Z.C.; Liu, C.J.; Chen, Y.X.; Chen, G.C.; Hu, N.; Gao, F. Sediment Source Analysis for the Maerzheng Formation Sandstone in Gerizhuotuo Area, Southern Margin of East Kunlun Region: Evidence for Detrital Zircon U–Pb Geochronology. *Acta Geol. Sin.* **2017**, *91*, 1326–1344.
25. Wu, C.; Andrew, V.Z.; Chen, X.H.; Ding, L.; Drew, A.L.; Liu, C.F.; Liu, W.C.; Jiang, T.; Daniel, F.S. Tectonics of the Eastern Kunlun Range: Cenozoic Reactivation of a Paleozoic–Early Mesozoic Orogen. *Tectonics* **2018**, *38*, 1609–1650. [CrossRef]
26. Wu, R.C.; Gu, X.X.; Zhang, Y.M.; He, L.; Kang, J.Z.; Yu, F.C.; Feng, L.Q.; Xu, J.C. The Sedimentary Geochemical Records about the Tectonic Evolution of the East Kunlun Orogenic Belt from Early Paleozoic to Early Mesozoic. *Geoscience* **2017**, *31*, 716–733.
27. Yu, M.; Dick, J.M.; Feng, C.Y.; Li, B.; Wang, H. The tectonic evolution of the East Kunlun Orogen, northern Tibetan Plateau: Acritical review with an integrated geodynamic model. *J. Asian Earth Sci.* **2020**, *191*, 104–168. [CrossRef]
28. Pei, X.Z.; Li, R.B.; Li, Z.C.; Liu, C.J.; Chen, Y.X.; Pei, L.; Liu, Z.Q.; Chen, G.C.; Li, X.B.; Wang, M. Composition Feature and Formation Process of Buqingshan Composite Accretionary Mélange Belt in Southern Margin of East Kunlun Orogen. *Earth Sci.* **2018**, *43*, 4498–4520.
29. Chen, N.S.; Sun, M.; Wang, Q.Y.; Zhang, K.X.; Wan, Y.S.; Chen, H.H. U–Pb dating of zircon from the central zone of the East Kunlun Orogen and its implications for tectonic evolution. *Sci. China Ser. D* **2008**, *6*, 657–666. [CrossRef]
30. Meng, F.C.; Cui, M.H.; Wu, X.K.; Wu, J.F.; Wang, J.H. Magmatic and metamorphic events recorded in granitic gneisses from the Qimantag, East Kunlun Mountains, Northwest China. *Acta Petrol. Sin.* **2013**, *29*, 2107–2122.
31. He, D.F.; Dong, Y.P.; Liu, X.M.; Yang, Z.; Sun, S.S.; Cheng, B.; Li, W. Tectono–thermal events in East Kunlun, Northern Tibetan Plateau: Evidence from zircon U–Pb geochronology. *Gondwana Res.* **2016**, *30*, 179–190. [CrossRef]
32. Mo, X.X.; Luo, Z.H.; Deng, J.F.; Yu, X.G.; Liu, C.D.; Shen, H.W.; Yuan, W.M.; Liu, Y.H. Granitoids and Crustal Growth in the East–Kunlun Orogenic Belt. *J. China Univ. Geosci.* **2007**, *13*, 403–414.
33. Chen, Y.X.; Pei, X.Z.; Li, Z.C.; Li, R.B.; Liu, C.J.; Chen, G.C.; Pei, L.; Wei, B. Geochronology, geochemical features and geological significance of the granitic gneiss in Balong area, East Section of East Kunlun. *Acta Petrol. Sin.* **2015**, *31*, 2230–2244.
34. Jiang, C.F.; Feng, B.G.; Yang, J.S.; Zhu, Z.Z.; Zhao, M.; Chai, Y.C.; Shi, X.D.; Hu, J.Q. An outline of the geology and tectonics of the Kunlun Mts. *area. Bulletin Inst. Geol. Chin. Acad. Geol. Sci.* **1986**, *15*, 70–79.
35. Xiong, F.H.; Ma, C.Q.; Wu, L.; Jiang, H.G.; Liu, B. Geochemistry, zircon U–Pb ages and Sr–Nd–Hf isotopes of an Ordovician appinitic pluton in the East Kunlun orogen: New evidence for Proto–Tethyan subduction. *J. Asian Earth Sci.* **2015**, *111*, 681–697. [CrossRef]
36. Chen, Y.X.; Pei, X.Z.; Li, R.B.; Liu, Z.Q.; Li, Z.C.; Zhang, X.F.; Chen, G.C.; Liu, Z.G.; Ding, S.P.; Guo, J.F. Zircon U-Pb age of Xiaomiao Formation of Proterozoic in the eastern section of the East Kunlun Orogenic Belt. *Geoscience* **2011**, *25*, 510–521.
37. Chen, Y.X.; Pei, X.Z.; Li, R.B.; Li, Z.C.; Pei, L.; Liu, Z.Q.; Chen, G.C.; Liu, C.J.; Yang, J. Association, geochemical characteristics and tectonic setting of the Xiaomiao Formation, east region of East Kunlun Orogenic Belt. *Acta Geol. Sin.* **2014**, *88*, 1038–1054.
38. Chen, G.C.; Pei, X.Z.; Li, R.B.; Li, Z.C.; Liu, C.J.; Chen, Y.X.; Pei, L.; Ding, S.P. Geological Characteristics and Tectonic Significance of Jurassic Yangqu Formation from Alake Lake in the Eastern Part of East Kunlun Orogenic Belt. *N. Geol.* **2017**, *50*, 113–125.
39. Wu, N.Y.; Wang, M.Q. The Carboniferous system and its fossil assemblage characteristics in Northern Xinjiang. *Xinjiang Geol.* **1983**, *2*, 17–31.
40. Li, J.C.; Kuang, D.Z.; Zhang, Z.H.; Hong, Z.Y. Late Carboniferous-early Permian Fusulinid Biostratigraphy of Shunchuang, Fujian Province. *Acta Micropalaeontologica Sin.* **2011**, *28*, 60–66.
41. Liu, Y.S.; Liu, X.M.; Hu, Z.C.; Diwu, C.R.; Yuan, H.L.; Gao, S. Evaluation of accuracy and long–term stability of determination of 37 trace elements in geological samples by ICP–MS. *Acta Petrol. Sin.* **2007**, *23*, 1203–1210.
42. Zong, K.Q.; Klemd, R.; Yuan, Y.; He, Z.Y.; Gao, J.L.; Shi, X.L.; Liu, Y.S.; Hu, Z.C.; Zhang, Z.M. The Assembly of Rodinia: The Correlation of Early Neoproterozoic (ca. 900 Ma) High–Grade Metamorphism and Continental Arc Formation in the Southern Beishan Orogen, Southern Central Asian Orogenic Belt (CAOB). *Precambrian. Res.* **2017**, *290*, 32–48. [CrossRef]
43. Yan, Z.; Wang, Z.Q.; Chen, J.L.; Yan, Q.R.; Wang, T. Detrital record of Neoproterozoic arc-magmatism along the NW margin of the Yangtze Block, China: U-Pb geochronology and petrography of sandstones. *J. Asian Earth Sci.* **2010**, *37*, 322–334. [CrossRef]

44. Sun, S.S.; Mc Donough, W.F. Chemical and isotopic systematics of oceanic basalts: Implications for mantle composition and processes. *Geol. Soc. Spec. Publ.* **1989**, *42*, 313–345. [CrossRef]
45. Taylor, S.R.; McLenana, S.M. *The Continental Crust: Its Composition and Evolution*; Oxford Blackwell: Oxford, UK, 1985; pp. 1–312.
46. Hoskin, P.W.O.; Schaltegger, U. The composition of zircon and igneous and metamorphic petrogenesis. *Rev. Mineral. Geochem.* **2003**, *53*, 27–62. [CrossRef]
47. Blank, L.P.; Kamo, S.L.; Williams, I.S.; Mundil, R. The application of SHRIMP to Phanerozoic geochronology: A critical appraisal of four zircon Standards. *Chem. Geol.* **2003**, *200*, 171–188.
48. Gehrels, G.E.; Johnsson, M.J.; Howell, D.G. Detrital zircon geochronology of the Adams Argillite and Nation River Formation, east–central Alaska, USA. *J. Sediment. Res.* **1999**, *69*, 135–144. [CrossRef]
49. Sircombe, K.N. Tracing Provenance through the Isotope Ages of Littoral and Sedimentary Detrital Zircon, Eastern Australia. *Sediment. Geol.* **1999**, *124*, 47–67. [CrossRef]
50. Nesbitt, H.W.; Young, G.M. Prediction of some weathering trends of plutonic and volcanic rocks based on thermodynamic and kinetic considerations. *Geochim. Cosmochim. Acta* **1984**, *48*, 1523–1534. [CrossRef]
51. Fedo, C.M.; Nesbitt, H.W.; Young, G.M. Unraveling the effects of potassium metasomatism in sedimentary rocks and paleosols, with implications for paleo weathering conditions and provenance. *Geology* **1995**, *23*, 921–924. [CrossRef]
52. Zhang, B.; Cheng, W.; Zhang, Q.; Li, Y.; Sun, P.; Fathy, D. Occurrence Patterns and Enrichment Influencing Factors of Trace Elements in Paleogene Coal in the Fushun Basin, China. *ACS Earth Space Chem.* **2022**, *6*, 3031–3042. [CrossRef]
53. Bock, B.; Mc Lennan, S.M.; Hanson, G.N. Geochemistry and provenance of theMiddle Ordovician Austin Glen Member (Normanskill Formation) and the TaconianOrogeny in New England. *Sedimentology* **1998**, *45*, 635–655. [CrossRef]
54. Gromet, L.P.; Haskin, L.A.; Korotev, R.L.; Dymek, R.F. The "North American shale composite": Its compilation, major and trace element characteristics. *Geochim. Cosmochim. Acta* **1984**, *48*, 2469–2482. [CrossRef]
55. Condie, K.C. Chemical composition and evolution of the upper continental crust: Contrasting results from surface samples and shales. *Chem. Geol.* **1993**, *104*, 1–37. [CrossRef]
56. McLennan, S.M. Relationship between the trace element composition of sedimentary rocks and upper continental crust. *Geochem. Geophys. Geosysystem* **2001**, *2*, 203–236. [CrossRef]
57. Nesbitt, H.W.; Young, G.M. Formation and diagenesis of weathering profile. *J. Geol.* **1989**, *97*, 129–147. [CrossRef]
58. Hayashi, K.I.; Fujisawa, H.; Holland, H.D.; Ohmoto, H. Geochemistry of ~1.9 Gasedimentary rocks from northeastern Labrador, Canada. *Geochim. Cosmochim. Acta* **1997**, *61*, 4115–4137. [CrossRef]
59. Shi, Y.; Huang, Q.W.; Liu, X.J.; Krape, B.; Yu, J.H.; Bai, Z.A. Provenance and tectonic setting of the supra–crustal succession of the Qinling complex: Implications for the tectonic affinity of the north Qinling belt, central China. *J. Asian Earth Sci.* **2018**, *158*, 112–139. [CrossRef]
60. Fathy, D.; Wagreich, M.; Ntaflos, T.; Sami, M. Provenance Characterization of Campanian Lacustrine Organic-Rich Mudstones on the Southern Tethyan Margin, Egypt. *ACS Earth Space Chem.* **2021**, *5*, 197–209. [CrossRef]
61. Floyd, P.A.; Leveridge, B.E. Tectonic environment of the Devonian Gramscatho basin, south Cornwall: Framework mode and geochemical evidence from turbiditic sandstones. *Jour. Geol. Soc.* **1987**, *144*, 531–542. [CrossRef]
62. Belousova, E.A.; Griffin, W.L.; O'Reilly, S.Y.; Fisher, N. Igneous zircon: Trace element composition as an indicator of source rock type. *Contrib. Min. Petr.* **2002**, *143*, 602–622. [CrossRef]
63. Liu, H.Y.; McKenziea, N.R.; Colleps, C.L.; Chen, W.; Ying, Y.C.; Stocklid, L.; Sardsude, A.; Stockli, D.F. Zircon isotope–trace element compositions track Paleozoic–Mesozoic slab dynamics and terrane accretion in Southeast Asia. *Earth Planet Sci. Lett.* **2022**, *578*, 117298. [CrossRef]
64. Brennana, D.T.; Link, P.K.; Li, Z.X.; Martinc, L.; Johnsond, T.; Evanse, N.J.; Li, J.Y. Closing the "North American Magmatic" Gap: Crustal evolution of the Clearwater Block from multi-isotope and trace element zircon data. *Precambrian Res.* **2022**, *369*, 106533. [CrossRef]
65. Floyd, P.A.; Winchester, J.A.; Park, R.G. Geochemistry and tectonic setting of Lewisian clastic metasediments from the Early Proterozoic Loch Maree Group of Gairloch, NW Scotland. *Precambrian Res.* **1989**, *45*, 203–214. [CrossRef]
66. Roser, B.P.; Korsch, R.J. Provenance signatures of sandstone–mudstone suites determined using discriminant function analysis of major–Element data. *Chem. Geol.* **1988**, *67*, 119–139. [CrossRef]
67. Bhatia, M.R.; Crook, K.A.W. Trace element characteristics of graywackes and tectonic setting discrimination of sedimentary basins. *Contrib. Min. Petr.* **1986**, *92*, 181–193. [CrossRef]
68. Feng, D.; Wang, C.; Song, S.G.; Xiong, L.; Zhang, C.B.; Mark, B.A.; Dong, J.; Wen, T.; Su, L. Tracing tectonic processes from Proto– to Paleo–Tethys in the East Kunlun Orogen by detrital zircons. *Gondwana Res.* **2023**, *115*, 1–6. [CrossRef]
69. Xin, W.; Sun, F.Y.; Zhang, Y.T.; Fan, X.Z.; Wang, Y.C.; Li, L. Mafic–intermediate igneous rocks in the East Kunlun Orogenic Belt, northwestern China: Petrogenesis and implications for regional geodynamic evolution during the Triassic. *Lithos* **2019**, *346–347*, 105159. [CrossRef]
70. Sun, L.; Wang, W.; Manoj, K.P.; Lu, G.M.; Xue, E.K.; Huang, B.; Zhang, Y.; Jin, W.; Tian, Y. Geochemical and detrital zircon age constraints on Meso– to Neoproterozoic sedimentary basins in the southern Yangtze Block: Implications on Proterozoic geodynamics of South China and Rodinia configuration. *Precambrian Res.* **2022**, *378*, 106779. [CrossRef]
71. Cawood, P.A.; Hawkesworth, C.J.; Dhuime, B. Detrital zircon record and tectonic setting. *Geology* **2012**, *40*, 875–878. [CrossRef]

72. Liu, Z.Q.; Pei, X.Z.; Li, R.B.; Li, Z.C.; Zhang, X.F.; Liu, Z.G.; Chen, G.C.; Chen, Y.X.; Ding, S.P.; Guo, J.F. LA-ICP-MS Zircon U-Pbgeochronology of the two suites of ophiolites at the Buqingshan area of the A'nyemaqen Orogenic Belt in the southern margin ofEast Kunlun and its tectonic implication. *Acta Geol. Sin.* **2011**, *85*, 185–194.
73. Chen, L.; Sun, Y.; Pei, X.Z.; Feng, T.; Zhang, G.W. Comprehensive correlation of Paleo-Tethys ophiolite and its dynamic significance:A case study of Derrni ophiolite. *Sci. China Ser. D* **2003**, *33*, 1136–1142.
74. Yang, J.S.; Wang, X.B.; Shi, R.D.; Xu, Z.Q.; Wu, C.L. The Dur'ngoi ophiolite in East Kunlun, northern Qinghai-Tibet Plateau: Afragment of paleo-Tethyan oceanic crust. *Geol. China* **2004**, *31*, 225–239.
75. Roger, F.; Arnaud, N.; Gilder, S.; Tapponnier, P.; Jolivet, M.; Brunel, M.; Malavieille, J.; Xu, Z.Q.; Yang, J.S. Geochronological andgeochemical constraints on Mesozoic suturing in east central Tibet. *Tectonics* **2003**, *22*, 1037. [CrossRef]
76. Li, C. A review on 20 Years' Study of the Longmu Co-Shuanghu-Lancang River Suture Zone in Qinghai-Xizang (Tibet) Plateau. *Geol. Rev.* **2008**, *54*, 105–119.
77. Zhai, Q.G.; Jahn, B.M.; Wang, J.; Hu, P.Y.; Chung, S.L.; Lee, H.Y.; Tang, S.H.; Tang, Y. Oldest Paleo-Tethyan ophiolitic mlange inthe Tibetan Plateau. *Geol. Soc. Am. Bull.* **2016**, *128*, 355–373. [CrossRef]
78. Zuza, A.V.; Yin, A. Balkatach hypothesis: A new model for the evolution of the Pacific, Tethyan, and Paleo-Asian oceanic domains. *Geosphere* **2017**, *13*, 1664–1712. [CrossRef]
79. Wang, Y.; Qian, X.; Cawood, P.A.; Liu, H.; Feng, Q.; Zhao, G.; Zhang, Y.; He, H.; Zhang, P. Closure of the East PaleotethyanOcean and amalgamation of the Eastern Cimmerian and Southeast Asia continental fragments. *Earth Sci. Rev.* **2018**, *186*, 195–230. [CrossRef]
80. Xiao, W. Accretionary Tectonics of the Western Kunlun Orogen, China: A Paleozoic-Early Mesozoic, Long-Lived ActiveContinental Margin with Implications for the Growth of Southern Eurasia. *J. Geol.* **2005**, *113*, 687–705. [CrossRef]
81. Metcalfe, I. Gondwana dispersion and Asian accretion: Tectonic and Paleogeographic evolution of eastern Tethys. *J. Asian Earth Sci.* **2013**, *66*, 1–33. [CrossRef]
82. Metcalfe, I. Tectonic evolution of the Malay Peninsula. *Asian Earth Sci.* **2013**, *76*, 195–213. [CrossRef]

Disclaimer/Publisher's Note: The statements, opinions and data contained in all publications are solely those of the individual author(s) and contributor(s) and not of MDPI and/or the editor(s). MDPI and/or the editor(s) disclaim responsibility for any injury to people or property resulting from any ideas, methods, instructions or products referred to in the content.